Research on die-less spinning by spherical roller of different radius

Shuyang Zhou[1] · Zhiren Han[1,2] ⬤ · Zhen Jia[2] · Baoming Liu[2] · Xue Gong[2]

Abstract

Die-less spinning is developed because of its advantages of low cost and high flexibility. The spherical roller has not been commonly used in the die-less spinning process. In previous studies, the sizes of the spherical rollers are varied, and the distributions of the wall thickness of the formed parts are inconsistent. To explore the effects of spherical roller dimensions on the formed parts, four spherical rollers of different radii are adopted to form the truncated cone-shaped parts. Meanwhile, the finite element models are established to analyze the stress states during the spinning process. The wall thickness distribution and the outer contour accuracy of the experimental parts are measured. Combined with the finite element simulation results, it is found that the curvature of the roller and the contact area between the roller and the sheet has an important influence on the wall thickness distribution and outer contour accuracy of the parts. In addition, the too-small radius of the roller makes the shear stress on the sheet material greatly increase. It results in the wall consistent with the sin law of die-less shear spinning.

1 Introduction

Metal spinning is a widely used forming process. It has several advantages such as flexibility, low cost, and high-quality surface finish of formed parts [1]. With the development of spinning technology, die-less spinning has replaced die spinning to form parts of many shapes. The shape of the spinning roller has also become diverse [2].

The spherical roller was not commonly used in the spinning process. A cone-shaped roller whose roller angle can change in three directions was used by Elkhabeery et al. [3] to investigate the effect of spinning parameters on the wall thickness, spinning ratio, etc. of the cups. They found that the increasing roller nose radius caused an increase in the roller-work contact area and a lower stress concentration in the deformation zone. This eventually led to an increase in wall thickness with the increase in cup height. Xia et al. [4] studied the one-path deep drawing spinning of cups by using a roller whose profile was an arc with a constant radius. By measuring the radial and axial components of the spinning force during the forming process, they explained that the wall of the cup edge was thicker than the original one due to the previous deep drawing. Sekiguchi et al. [5] formed curved products with a spherical head roller whose radius was 8 mm. The size of the roller is much smaller than the size of the roller Xia used. And the wall thickness of formed parts basically conformed to the sin law. Later, they studied an oblique shear spinning method to control the wall thickness distribution of the formed parts [6]. They controlled the wall thickness distribution by inclining the flange plane of the part during spinning. When the inclination angle of the flange plane was larger, the wall of the part was thicker. But it can not be thicker than the initial wall thickness. In recent years, Jia et al. [7, 8] studied die-less spinning by a ball-crown-shaped roller whose radius was 35 mm. Whether the formed part was a cone-cylinder shape or a cone shape, its wall was thicker than the initial sheet. They observed the microstructure of the part and detected the residual stress. The thickening of the part wall was caused by the material accumulation in the circumferential direction and the weakening of material pulled out by the ball-crown-shaped roller. Obviously, the size of the spherical roller affects the wall thickness of the formed parts.

✉ Zhiren Han
  hanren888@163.com

1 School of Mechanical Engineering, Northwestern Polytechnical University, Xi'an 710072, China

2 Key Lab of Fundamental Science for National Defense of Aeronautical Digital Manufacturing Process, Shenyang Aerospace University, Shenyang 110136, China

The spherical roller was not only used in the spinning process but was also applied in the incremental sheet forming. Spinning and incremental sheet forming are similar technologies. They have the same relative motion relationship between the sheet and the tool. In incremental forming, variable shapes and dimensions of the tools were applied to test if the formability limit changed from fracture to necking [9]. Kumar et al. [10] formed the truncated cone-shaped parts to study the influence of tool diameter on the forming depth. The diameter of the tools they used ranged from 7.52 to 15.66 mm. The results showed that formability decreased with the decrease in tool diameter. It also showed the effect of the tool diameter on the forming parts.

In this paper, the effects of spherical roller dimensions on the formed parts are explored. The reason for these effects is investigated. Section 2 describes the roller device and the calculation method of the roller path for the truncated cone-shaped part. Section 3 introduces the experimental conditions and results. Section 4 presents the process and results of finite element simulation in ABAQUS software. And in the next section, the phenomenon and results are discussed. Finally, the conclusion is summarized.

2 Roller

2.1 Roller device

A roller device was designed to simplify the process of roller replacement and save the cost as shown in Fig. 1. The spherical roller is bolted to one end of the mandrel. The mandrel is fitted with two thrust bearings so that it can rotate on the roller holder. A nut is attached to the other end of the mandrel to ensure that the mandrel does not bounce around on the roller holder. When replacing the roller, just remove the mandrel from the roller holder and loosen the bolt. This device can be fitted with spherical rollers of various sizes.
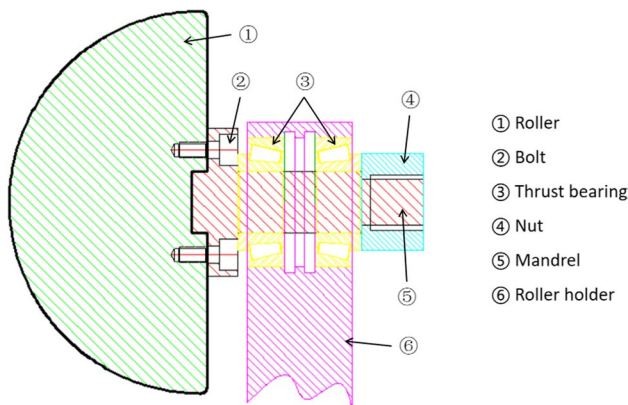

① Roller
② Bolt
③ Thrust bearing
④ Nut
⑤ Mandrel
⑥ Roller holder

**Fig. 1** Sectional view of roller device

2.2 Roller path

The paths of the spherical rollers are different for different diameters. But their calculation methods are consistent. As mentioned in Zhou's paper [11], the position of the tangential circle on the spherical roller is important in roller path calculation. The same is true for the truncated cone-shaped part spinning. In the calculation of the roller path, the position of the tangent circle corresponds to the half-cone angle of the forming part. According to the calculations in Zhou's paper, the half-cone angle of the forming part and the angle between the roller axis and the line connecting the center of the sphere and the tangential circle are congruent with each other. Therefore, the smaller the half-cone angle of the forming part, the closer the position of the tangential circle is to the bottom section of the spherical roller. During the spinning process, the sheet may wrap the field from the tangential circle to the top of the spherical roller, while the area from the tangential circle to the bottom section of the spherical roller is never in contact with the sheet. So the shorter the height of the spherical roller, the smaller the range of half-cone angles it can form the part. When the height of the spherical roller is too short and the half-cone angle of the forming part is too small, as shown in Fig. 2a, it results in the tangential circle out of the spherical roller. In this case, the roller path should be recalculated, and the corresponding half-cone angle of the part can be shaped by the contact of the rounded surface on the roller between the spherical surface and the bottom section, as shown in Fig. 2b. This case belongs to spherical variable curvature forming and is not considered in this paper.

Since the spherical roller has a large contact area with the sheet during the spinning process, it is inappropriate to take a point on the sphere as the reference point of the roller in the calculation of the roller path. The center of the sphere is the most suitable reference point for the spherical roller. The distance of any point on the sphere from its center is its radius. It is convenient for path calculation. For a truncated cone-shaped part with a constant half-cone angle, the roller path is a straight line. Figure 3 shows the sketch of the roller path calculation. The top center of the mandrel is set to the origin. As shown in Fig. 3a, the equations for calculating the spherical center position of the roller at the start of spinning are as follows

$$X_{cs} = \left(R + t_0 + r\right) \times tan\left(\frac{\beta}{2}\right) + \frac{D_0}{2} - r \tag{1}$$

$$Z_{cs} = -\left(t_0 + R\right) \tag{2}$$

Fig. 2 Schematic diagram of small half-cone angle part formed by spherical roller with short height. **a** Tangential circle out of spherical roller. **b** Roller path recalculated
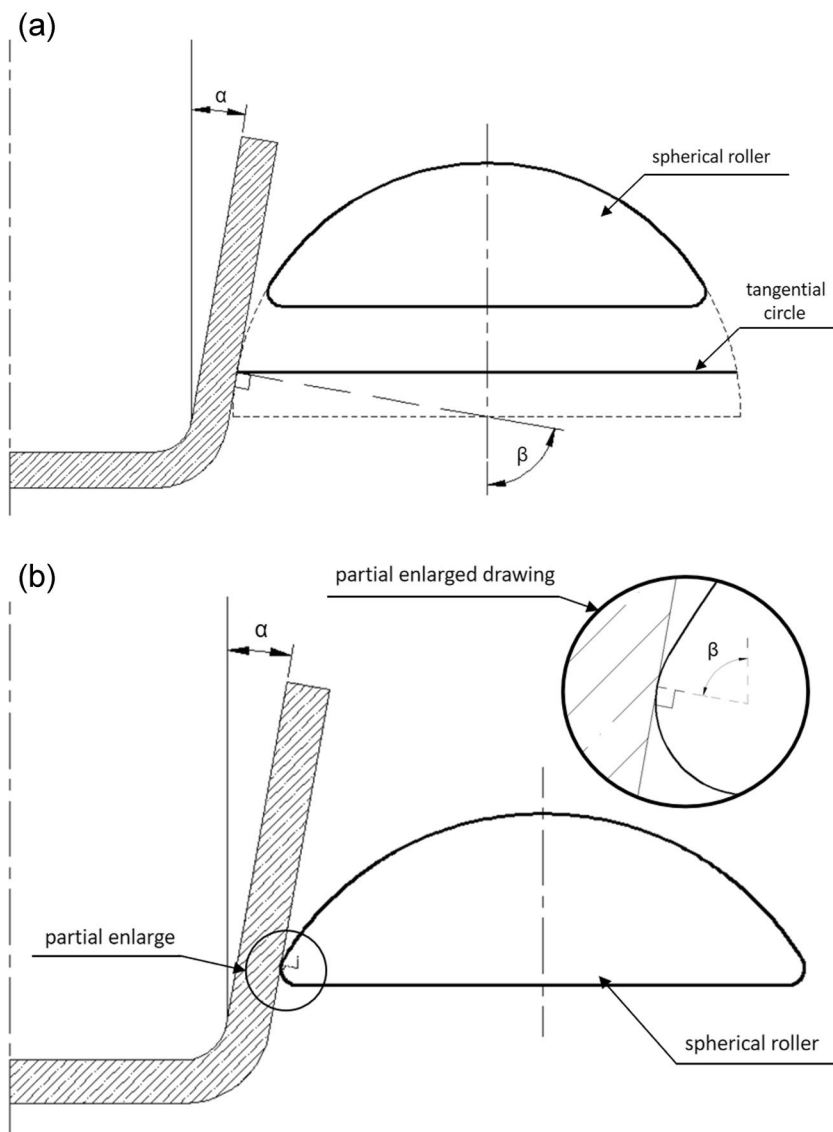
where R denotes the radius of the spherical roller. t_0 denotes the initial thickness of the sheet. r denotes the radius of the mandrel shoulder. β denotes the angle between the roller axis and the line which connecting the center of sphere and the tangential circle. D_0 denotes the diameter of the mandrel.

As shown in Fig. 3b, the equations for calculating the spherical center position of the roller at the end of spinning are as follows

$$X_{ce} = \frac{D_0}{2} - r + (r + t_0) \times sin\beta + L \times sin\alpha + R \times sin\beta \quad (3)$$

$$Z_{ce} = r - (r + t_0) \times cos\beta + L \times cos\alpha - R \times cos\beta \quad (4)$$

where α denotes the half-cone angle of the forming part. L denotes the predicted generatrix length of the truncated cone-shaped part. Since the generatrix length is predicted,

this value is generally larger in order to ensure that the part is fully shaped.

3 Experiment

3.1 Experimental conditions

The spinning experiments performed by the PS-CNC-SXY600-5 spinning machine is shown in Fig. 4. The roller is driven by two independent servomotors, one of which controls the axial feed and the other controls the radial feed. The positioning accuracy and repeatability of the roller are as high as 0.025 mm. As shown in Fig. 5, four spherical rollers of different diameters were used in the experiments. Their dimensions are shown in Table 1. Where the heights of Roller #1 and Roller #4 are smaller than their radii, while

Fig. 3 Sketch of the roller path calculation. **a** Sketch of the spherical center position at the start of spinning. **b** Sketch of the spherical center position at the end of spinning
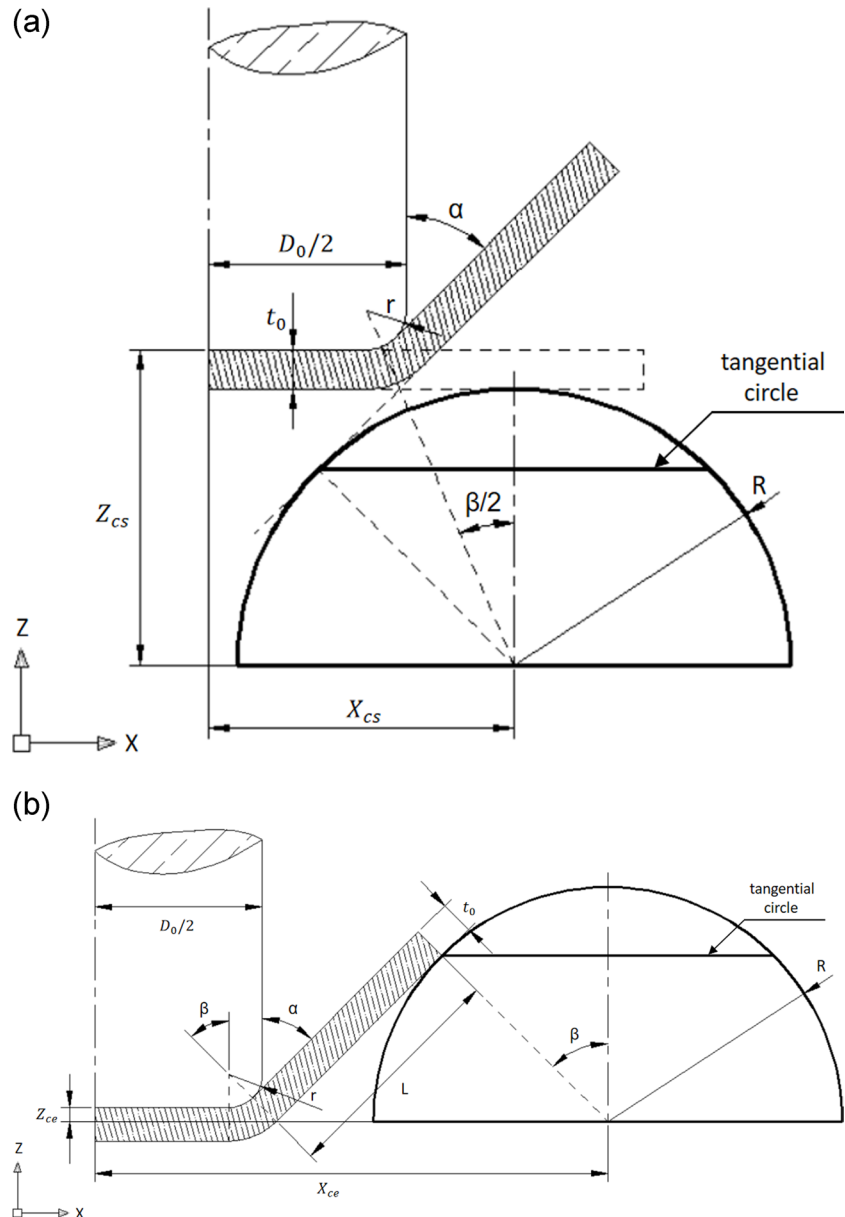
(a)

(b)

Fig. 4 PS-CNCSXY600-5 spinning machine

the heights of Roller #2 and Roller #3 are the same as their radii. Due to the large half-cone angle of the forming parts, the short heights of Roller #1 and Roller #4 do not affect the part forming according to the instruction in subsection 2.2.

In previous studies, the wall thickness of the part was affected by the diameter of the sheet. So two experimental working conditions were applied to investigate this effect. As shown in Table 2, the diameter of the sheets in Working condition A is 90 mm, while the diameter of the sheets in Working condition B is 140 mm. When the diameter of the sheets is 140 mm, according to the calculation of the roller path, the top of all spherical rollers is wrapped in sheet material for most of the spinning process. The opposite is the case when the sheet diameter is 90 mm. By comparing the parts formed under these two working conditions, the

Fig. 5 Spherical rollers with different dimensions

Table 1 Dimensions of spherical rollers

No.	Diameter (mm)	Height (mm)
1	35	25
2	62	62
3	70	70
4	85	30

Table 2 Working conditions

No.	Sheet diameter (mm)	Half-cone angle of part (°)
A	90	60
B	140	60

correlation between the sheet diameter and the roller radius can be explored.

3.2 Experimental results

The wall thickness of the parts along the cone wall was measured by a micrometer with an accuracy of 0.01 mm. The positions of the measuring points are shown in Fig. 6. The wall thickness ratios (t/t_0) of each part under Working condition A are shown in Fig. 7a. And the wall thickness ratios (t/t_0) of each part under Working condition B are shown in Fig. 7b.

The accuracy rating for the outer contour of the part along the cone wall was measured by a vernier caliper with an accuracy of 0.02 mm. The accuracy ratings for the outer contour of each part under Working condition A are shown in Fig. 8a. And the accuracy ratings for the outer contour of each part under

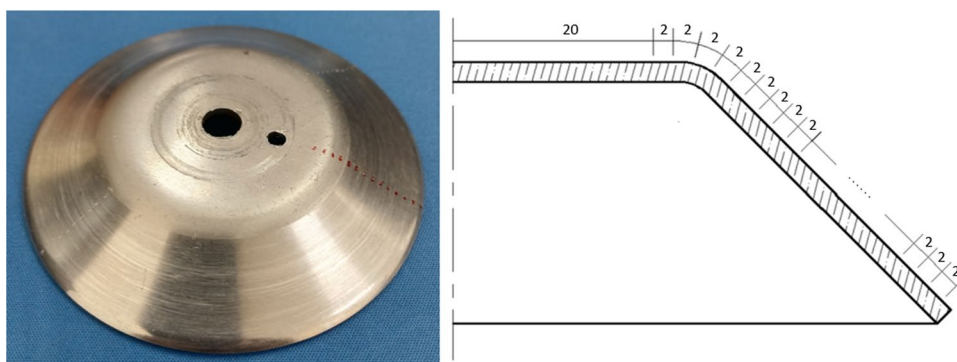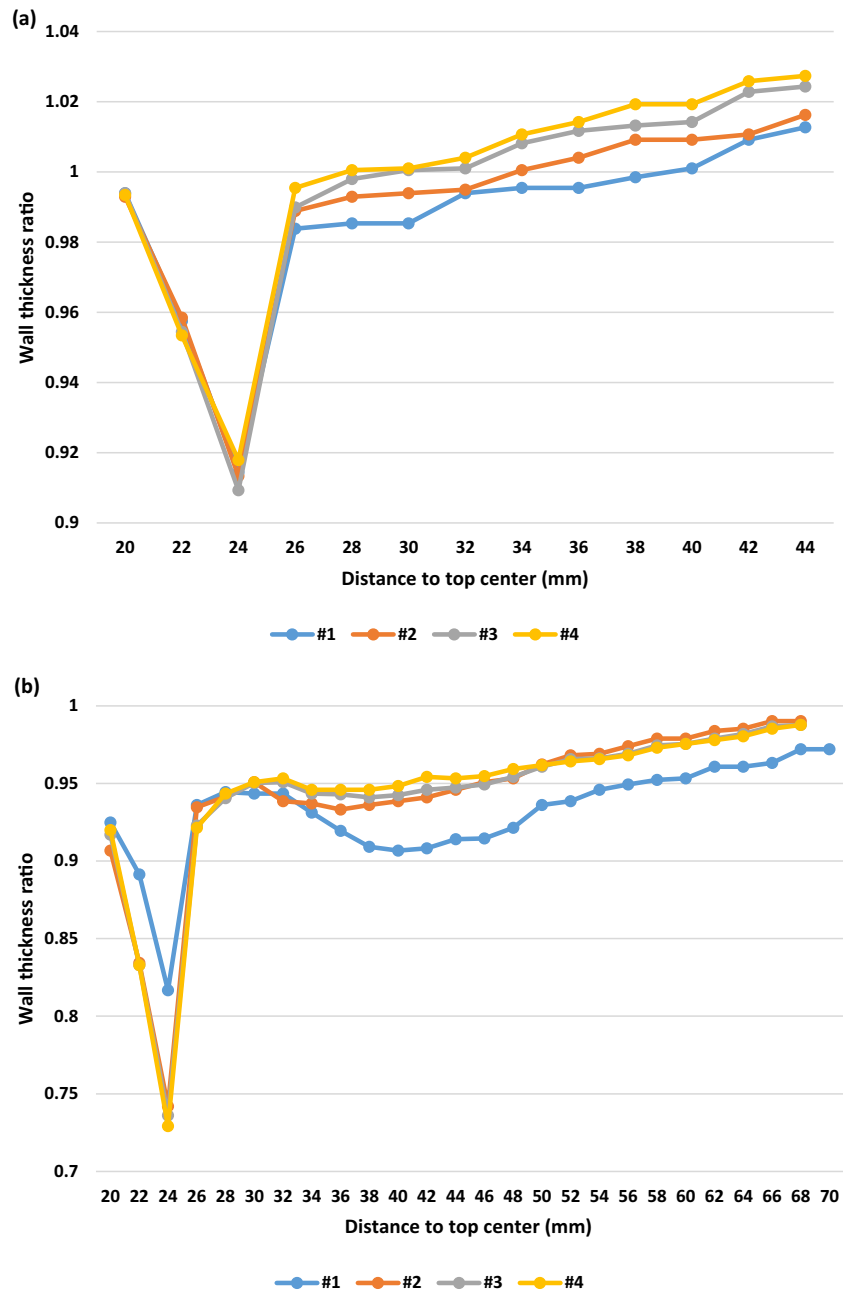**Fig. 6** Positions of measuring points on the part

Fig. 7 Line charts of the wall thickness ratios of the parts. **a** Working condition A. **b** Working condition B


4 Finite element analysis

Finite element analysis can help us understand more about the forces and flow of the material during the spinning process. The finite element models were established according to the experimental conditions in ABAQUS software. And the explicit finite element solution method was adopted to analyze the processes. The simulation parameters were consistent with those of the experimental working conditions. In addition, a spherical roller model of the same size as that mentioned in reference [6] was established to compare with these spherical rollers of larger radii.

4.1 Finite element model

The geometric model of the simulation was composed of the mandrel, spherical roller, and sheet as shown in Fig. 9. The

Working condition B are shown in Fig. 8b. The vertical axis of the line graph is the ratio of the distance of the actual part sidewall measurement point from the cone axis to the theoretical value. The horizontal axis of the line graph is the distance of the measurement point from the top center of the cone part.

Fig. 8 Line charts of the accuracy rating for the outer contour of the parts. **a** Working condition A. **b** Working condition B

(a)

(b)
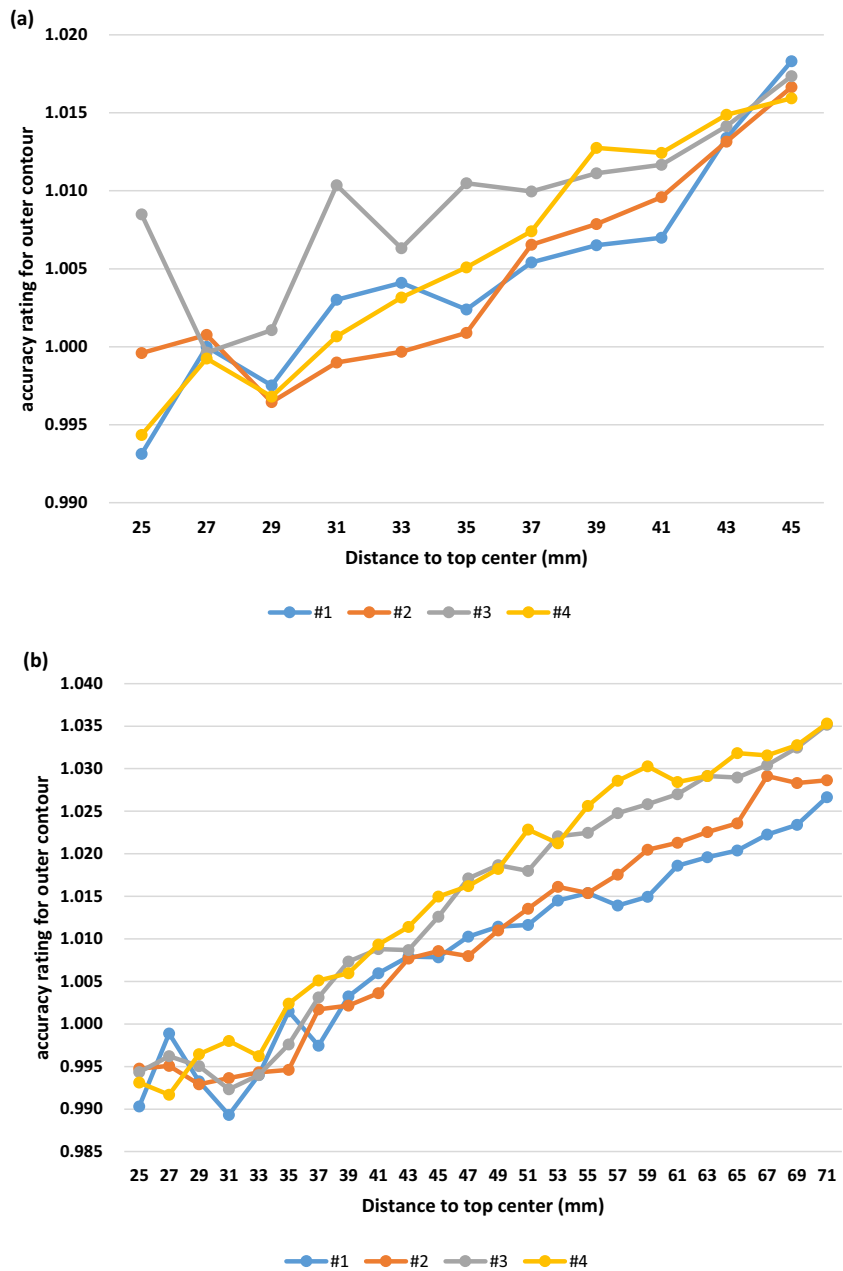
mandrel was simplified to a cylinder with a rounded shoulder. The spherical roller was simplified to a hemisphere. A hole was cut in the center of the sheet to facilitate meshing. The mandrel and the spherical roller were set to analytical rigid bodies, while the sheet was set as a deformable solid.

4.2 Material constitutive model

The sheet material used in experiments was 6061-O aluminum alloy. As shown in Table 3, its properties were consistent with those in Jia's paper [12]. The constitutive relation of the material was obtained from the following equation.

$$\sigma_f = 234\epsilon^{0.26} \tag{5}$$

where σ_f denotes the flow stress and ϵ denotes the true strain.

4.3 Other boundary conditions

A ring of material around the center hole of the sheet was tied to the mandrel to simplify the clamping device of the sheet. According to reference [12], the friction coefficient was set to the value of 0.15. The 8-node linear brick, reduced integration, and hourglass control element (C3D8R) was used to mesh the sheet. When the diameter of the sheet was 90 mm, the mesh was
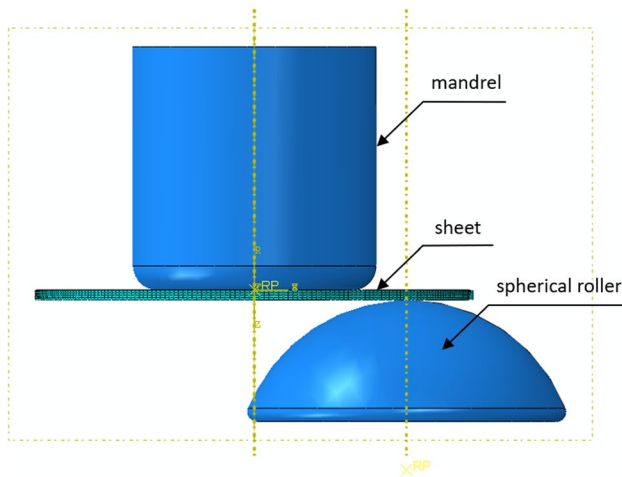
Fig. 9 Assembly diagram of the finite element model

Table 3 Material properties

Elastic modulus (MPa)	Poisson ratio	Yield strength (MPa)	Tensile strength (MPa)
67,000	0.33	51.59	146.12

divided into 4 layers along the thickness direction of the sheet. The total number of elements was about 43,000. For the sheet diameter of 140 mm, the 4-layer meshing method increased the number of elements exponentially and led to a long calculation time. So the mesh was divided into 2 layers along the thickness direction of the sheet. As a result, the total number of elements was about 60,000.

4.4 Simulation results

The simulations of all rollers under Working condition A were performed, while only the simulations of Roller #1 and Roller #3 under Working condition B were performed due to a long computation time. One of the simulation results was selected and compared with the experimental result to verify the reliability of the finite element results. Table 4 shows the errors between the simulation result and experimental result of the wall thickness of parts by Roller #1 under Working condition A. The maximum deviation is no more than 2.4%. In addition, the accuracy rating for the outer contour of the part was measured to compare the error between the simulation result and the experimental result. As shown in Table 5, the maximum deviation is 1.1%. These indicate that the finite element simulations for the spherical rollers are considered credible.

Table 4 Wall thickness ratio and error between simulation and experiment

Distance to top center (mm)	20	26	32	38	44
Experiment	0.994	0.984	0.994	0.998	1.013
Simulation	0.970	0.971	0.999	1.008	1.025
Error	−2.4	−1.3%	0.5%	1.0%	1.2%

5 Discussion

As shown in Fig. 7a, the wall thickness of the part thins as the roller radius decreases when the diameter of the sheet is 90 mm. This is especially true for the part sidewall. Theoretically, the larger the roller radius, the larger the contact area between the sheet and the roller will be. However, the diameter of the sheet limits the contact area between the large radius roller and the sheet material. Figure 10 shows the contact area between the sheet and Roller #1 and Roller #3 under Working condition A. It can be seen that their maximum contact areas are not very different. This does not affect their wall thickness too much. Yet, the smaller roller radius causes the sheet to be subjected to greater radial tensile stresses during the forming process. As shown in Fig. 11, the radial tensile stress caused by Roller #1 is larger than that caused by Roller #3 when they are forming the same field. A greater radial tensile stress leads to a thinner wall. This ultimately results in a thinner wall thickness for the part formed by the roller with a smaller radius when the diameter of the sheet is 90 mm.

When the diameter of the sheets is up to 140 mm, the wall thickness distributions of the parts are different. As shown in Fig. 7b, the wall thickness ratios are lower than 1. This indicates that a larger sheet diameter will subject the sheet material to greater radial tensile stresses during the spinning process. In addition, the wall of the part formed by Roller #1 is thicker than the others at the mandrel's shoulder. This is because the larger diameter of the sheet leads to a larger contact area between the roller and the sheet when the diameter of the sheets is large enough relative to the roller radius. Figure 12 shows the contact areas between the roller and the sheet during the spinning process. It can be seen that the maximum contact area of Roller #1 is about 20 mm^2, while the maximum contact area of Roller #3 is up to 35 mm^2 under Working condition B. A smaller contact area leads to a smaller resistance to deformation and friction from the material. And ultimately, it causes the wall of the part formed by Roller #1 at the mandrel's shoulder to be thicker than others. With the spinning process continuing, it can be seen from Fig. 12b, the contact area of Roller #3 begins to decline at about 10s. This is the time the tangent circle on Roller #3 just spun through the material at the mandrel's shoulder.

Table 5 Accuracy rating for the outer contour and error between simulation and experiment

Distance to top center (mm)	25	29	33	37	41	45
Experiment	0.993	0.998	1.004	1.005	1.007	1.018
Simulation	0.996	0.995	0.996	0.998	1.002	1.007
Error	0.3%	−0.3%	−0.8%	−0.7%	−0.5	−1.1%

Fig. 10 Contact area between roller and sheet under Working condition A
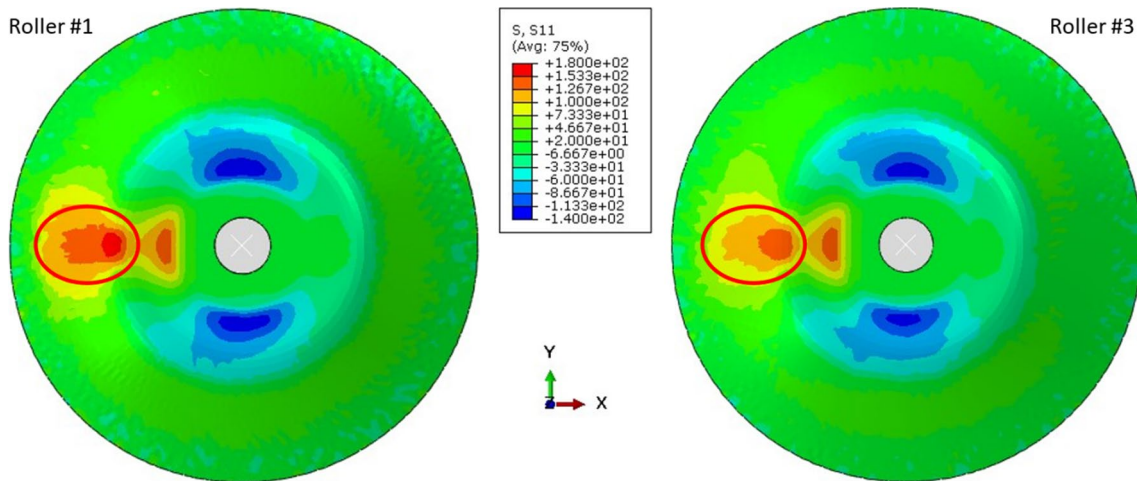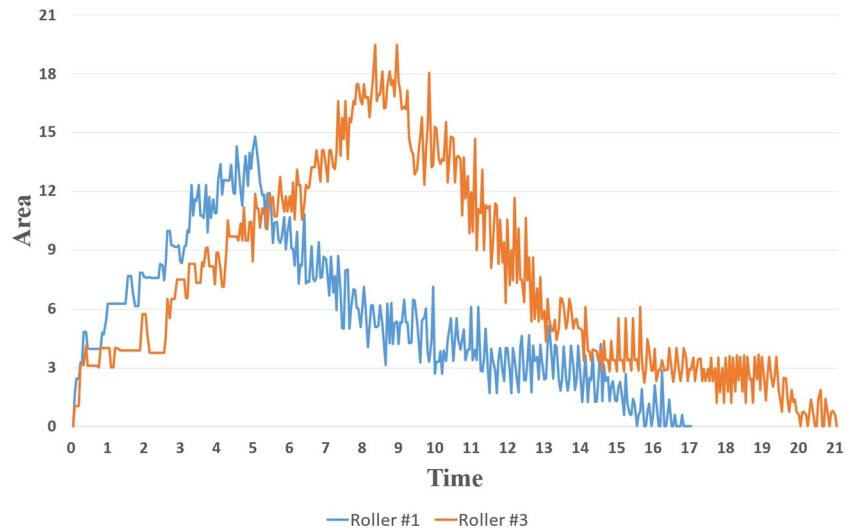
Fig. 11 Radial stress nephogram of the sheet performed by Roller #1 and Roller #3 under Working condition A

However, the contact area of Roller #1 is still maintained at a high level. After that, the wall of the part formed by Roller #3 begins to be thicker than that of the part formed by Roller #1.

It can be seen from Fig. 8 that the accuracy of the outer contour of the part is increasing with the cone height. This is mainly because the sheet is pushed and tilted due to the large axial force which is given by the roller during spinning.

However, the actual values of the outer contour at the mandrel's shoulder field are instead smaller than the theoretical values. The wall is thinning at the mandrel's shoulder field, but the theoretical values are calculated by the initial wall thickness. So the theoretical values of the outer contour at the mandrel's shoulder field are larger than the actual values. According to the line chart in Fig. 8b, the accuracy of the outer contour of the part formed by the roller with a

Fig. 12 Contact area between roller and sheet under Working condition B
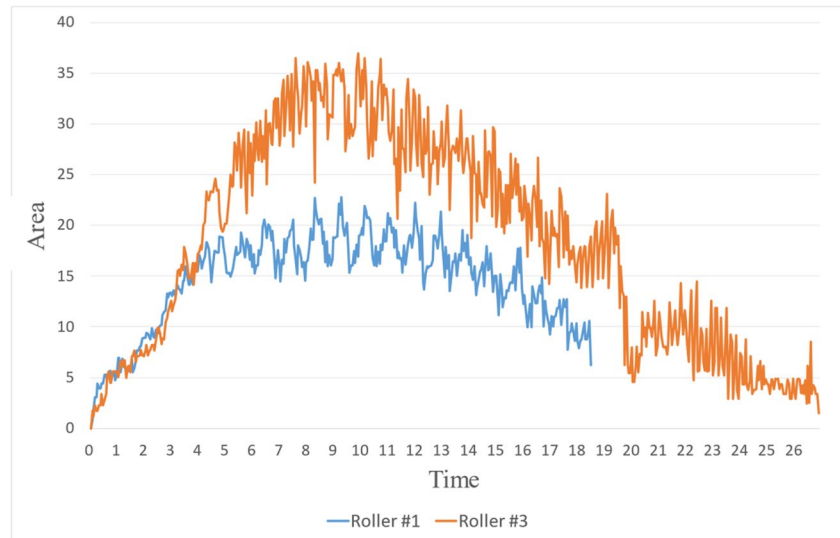
smaller radius is higher, while the line chart in Fig. 8a does not show a similar pattern. It is possible due to the contact area between the roller and the sheet. When the diameter of the sheet is 140 mm, the larger contact areas lead to greater resistance to deformation. These forces make the part more skewed during the spinning process and ultimately lead to poorer outer contour accuracy. When the diameter of the sheet is 90 mm, their contact areas do not differ much. So there is no significant difference in their outer contour accuracy.

A spherical roller model with an 8 mm radius was established and its simulation was performed. As reported in reference [6] and reference [7], the shapes of the spherical rollers they used are the same except for their radii. However, the wall thickness distributions of their parts are different. Figure 13a shows the shear stress in the direction of sheet thickness of the part formed by the roller of 8 mm radius. And Fig. 13b shows the shear stress in the direction of sheet thickness of the part formed by Roller #1. The diameters of their sheets are large enough that the contact area of Roller #1 is much larger than that of the other. However, the wall of the part formed by Roller #1 is thicker. It can be found that the sheet material suffers greater shear stress by the roller of 8 mm radius in the C region where the sheet is pushed down as shown in Fig. 13. This greater shear stress makes the wall consistent with the sin law of die-less shear spinning. While the shear stress on the sheet material formed by Roller #1 is several times smaller in the same position. The wall of the part is more like being pushed down. Its thickness does not decline a lot or even increase. The ratio factor between the thickness of the sheet and the radius of the roller is perhaps the key to whether the wall thickness is thinned or not.
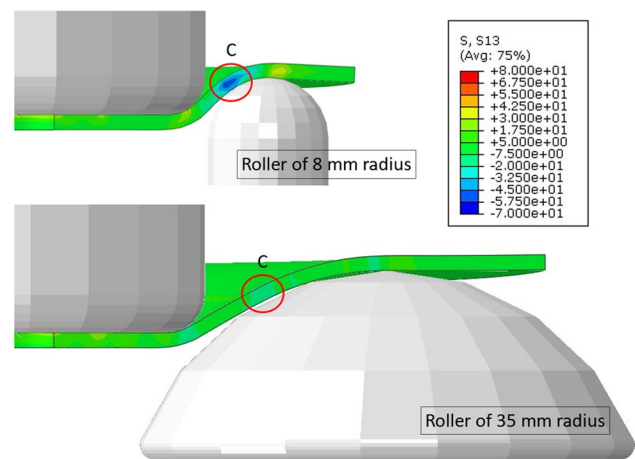

Fig. 13 Shear stress nephogram in sheet thickness direction performed by two sizes of rollers

6 Conclusions

(1) The calculation method of the roller path based on the spherical rollers is proposed. The equations for calculating the spherical center positions of the roller at the start and end of spinning are listed.

(2) When the diameter of the sheet is 90 mm, the sheet material is subjected to greater radial tensile stresses from the roller with a smaller radius. It leads to the wall getting thinner.

(3) When the diameter of the sheet is 140 mm, the spherical roller with a larger radius enlarges the contact area between the roller and the sheet. It results in greater resistance to deformation and friction from the material and the wall of the part getting thinner.

(4) The large axial force tilts the sheet during the spinning process so that the outer contour accuracy of the part decreases with the cone height. And larger contact area leads to greater resistance to deformation. These forces make the part more skewed and ultimately result in poorer outer contour accuracy.

(5) For a spherical roller with an 8 mm radius, the material suffers greater shear stress in the direction of sheet thickness at the top of the roller. It results in the wall consistent with the sin law of die-less shear spinning.

Declarations

Research involving humans and/or animals Not applicable.

Consent to participate The authors all approved to participate.

Consent for publication It is approved by all authors for publication.

Conflict of interest The authors declare no competing interests.

References

1. Music O, Allwood JM, Kawai K (2010) A review of the mechanics of metal spinning. J Mater Process Technol 210:3–23. https://doi.org/10.1016/j.jmatprotec.2009.08.021

2. Wong CC, Dean TA, Lin J (2003) A review of spinning, shear forming and flow forming processes. Int J Mach Tool Mamu 43:1419–1435. https://doi.org/10.1016/S0890-6955(03)00172-X

3. El-Khabeery MM, Fattouh M, El-Sheikh MN, Hamed OA (1991) On the conventional simple spinning of cylindrical aluminum cups. Int J Mach Tools Manuf 31(2):203–219. https://doi.org/10.1016/0890-6955(91)90005-N

4. Xia QX, Shima S, Kotera H, Yasuhuku D (2005) A study of the one-path deep drawing spinning of cups. J Mater Process Technol 159(3):397–400. https://doi.org/10.1016/j.jmatprotec.2004.05.027

5. Sekiguchi A, Arai H (2010) Synchronous die-less spinning of curved products. Steel Res Int 81(9):1010–1013

6. Sekiguchi A, Arai H (2012) Control of wall thickness distribution by oblique shear spinning methods. J Mater Process Technol 212(4):786–793. https://doi.org/10.1016/j.jmatprotec.2011.11.002

7. Jia Z, Ye T, Han ZR, Xiao Y, Ji SD (2019) Study on die-less spinning of cone-cylinder combined hollow parts. J Mater Process Technol 271:488–498. https://doi.org/10.1016/j.jmatprotec.2019.04.028

8. Jia Z, Bao HL, Gong X, Han ZR, Zhou SY, Ji SD (2021) Mechanical performance and microstructure of near-unthinned die-less spinning using ball-crown-shape roller. Int J Adv Manuf Technol 116(5):1667–1673. https://doi.org/10.1007/s00170-021-07571-9

9. Ben Said L (2022) The incremental sheet forming; technology, modeling and formability: a brief review. Proceedings of the Institution of Mechanical Engineers, Part E: Journal of Process Mechanical Engineering 236(6):2729–2755. https://doi.org/10.1177/09544089221093306

10. Kumar A, Gulati V, Kumar P, Singh V, Kumar B, Singh H (2019) Parametric effects on formability of AA2024-O aluminum alloy sheets in single point incremental forming. J Mater Res Technol 8(1):1461–1469. https://doi.org/10.1016/j.jmrt.2018.11.001

11. Zhou SY, Han ZR, Jia Z, Liu BM, Gong X (2022) Research on die-less spinning of square section cone by ball-crown-shape roller. Int J Adv Manuf Technol 121:1989–2003. https://doi.org/10.1007/s00170-022-09479-4

12. Jia Z, Han ZR, Liu BM, Xiao Y (2017) Work hardening of non-axisymmetric die-less spinning. J Mech Eng 63(2):111–118. https://doi.org/10.5545/sv-jme.2016.3589